ACS APPLIED MATERIALS & INTERFACES

www.acsami.org

Research Article

High-Quality-Factor AlON Transparent Ceramics for 5 GHz Wi-Fi Aesthetically Decorative Antennas

Chao Du, Di Zhou,* Shu-Zhao Hao, He-Tuo Chen,* Jian Zhang, Shi-Kuan Sun, Tao Zhou, Ming-Zhao Dang,* Shao-Fei Wang, Hai-Wen Liu, Long Li, and Zhuo Xu

Cite This: *ACS Appl. Mater. Interfaces* 2021, 13, 46866−46874

Read Online

ACCESS | Metrics & More | Article Recommendations

ABSTRACT: Transparent material has been widely used in product design and has seen a large increase in its use. In this paper, a kind of aesthetically decorative 5 GHz Wi-Fi dielectric resonator antenna (DRA) of aluminum oxynitride (AlON) transparent ceramic has been designed. High-quality-factor AlON transparent dielectric ceramics were fabricated by presintering at 1780 °C and further cold isostatic pressing (CIP) under a 200 MPa argon atmosphere. For a 9.0 mm thick specimen, the in-line light transmittance reached 83%. Optimum dielectric constant (ε_r = 9.32), quality factor (Qf = 47 960) and temperature coefficient (TCF = −51.7 ppm/°C) was achieved in the AlON transparent ceramic by cold isostatic pressing. As a result, the proposed aesthetically decorative DRA can achieve an impedance bandwidth of 32% (4.48−6.19 GHz), a high radiation efficiency of 85%, and a low cross-polarization discrimination (XPD) of −30 dB. To achieve a broad bandwidth, the proposed antenna was excited in its dominant TE^{x}_{111} mode and higher-order TE^{x}_{113} mode. The proposed antenna is thus an excellent candidate for an indoor decoration Wi-Fi antenna.

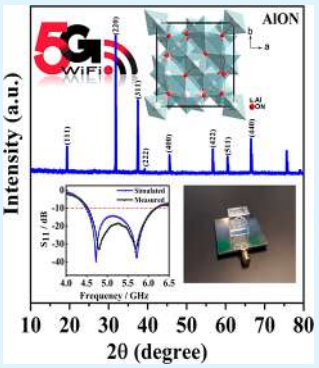

KEYWORDS: *microwave dielectric ceramics, dielectric resonator antenna, transparent ceramics, aesthetically decorative, indoor Wi-Fi*

INTRODUCTION

With the rapid progress in developing advanced smart home devices, indoor Wi-Fi devices are ubiquitous in modern urban spaces.[1] Sleeve antennas are attractive for indoor Wi-Fi wireless communication systems because they have simple structures and low cost.[2−4] However, the gain of a conventional sleeve antenna is relatively low, which limits the transmission range.[5] In addition, external sleeve antennas look unaesthetic and are contrary to the concept of a smart home. Therefore, the idea of designing an indoor aesthetically decorative Wi-Fi antenna with high gain and low loss is attractive.

It is well-known that the dielectric resonator antenna (DRA) was originally proposed by Long et al.[6] Compared with DRA, sleeve antennas with metallic structures as radiating elements suffer from low radiation efficiency due to ohmic losses that can be remedied by usage of a DRA.[7] DRAs have been proven to have superior properties such as small volume, lower loss, and easy excitation.[8,9] Most of the early investigations of the DRA were done for different applications. In 2012, as a special type of DRA, aesthetically decorative DRA was first proposed by Leung et al.[10] This idea was proved by using commercial transparent SiO_2 (ε_r = 7) glass decorations. Finally, the aesthetically decorative DRAs are excited in the broadside radiation modes using the aperture coupling feeding configuration excitation. In some applications, such as indoor Wi-Fi wireless communications, however, the index of refraction of transparent glass materials is generally less than 1.5, which is slightly worse for DRA applications.[11] In addition, the refractive index of transparent glass material is not a fixed constant, but has different values for different transmission wavelengths,[12] which is also a common concern of all antenna engineers.

Excellent dielectric properties of the dielectric resonator (DR) are required to make the prototype agree well with the simulated model. Compared with quartz glass, aluminum oxynitride (AlON) transparent ceramics possess low dispersion,[13] light weight,[14] high optical transmittance,[15] and outstanding mechanical properties.[16] Common transparent decorative materials such as plastic, glass, etc., are difficult to use in microwave devices because of their low dielectric constant and deteriorative dispersion.[11] At the same time, transparent crystals are difficult to use widely in microwave devices because they are difficult to process in large quantities. Figure 1 shows the performance characteristics of several transparent decorative materials. Because the resonance of electromagnetic waves in a DR occurs inside the ceramic dielectric material, the performance of AlON transparent ceramics material is subjected to the higher demands of suitable permittivity (ε_r), which can realize

Received: June 29, 2021
Accepted: September 13, 2021
Published: September 24, 2021

https://doi.org/10.1021/acsami.1c12223
ACS Appl. Mater. Interfaces 2021, 13, 46866−46874

Figure 1. Schematic diagram of the performance characteristics with different transparent decorative materials.

the broadband design of the DRA,[17] and must satisfy the manufacturing tolerances of the DRA as far as possible.[18] Higher quality factor ($Q = 1/\tan\delta$) can achieve a higher radiation efficiency of the DRA.[19] The dispersion effect, the relative permittivity of microwave dielectric ceramic materials, is a constant value in the microwave frequency band.[20] On the basis of the demands mentioned above, AlON transparent ceramics material is seen as a promising candidate in the design of the aesthetically decorative DRA. At present, AlON transparent ceramics have been widely applied in many fields, such as IR/visible windows,[21] electron microscope domes,[22] transparent armor,[23] and smartphone tablet panels.[24] Generally speaking, there are two manufacturing processes for obtain AlON transparent ceramics: a one-step synthesis method and a two-step synthesis method. For the one-step synthesis method, the raw materials are compacted directly and AlON transparent ceramics are synthesized through in situ reactions between the raw materials.[25,26] For the two-step synthesis method, AlON powders are first synthesized by the carbothermal reduction reaction of Al_2O_3 and AlN powders by plasma arc synthesis and self-propagation high-temperature synthesis. The as-prepared AlON powder is then used to produce AlON ceramics using pressureless sintering, hot pressing, and cold isostatic pressing (CIP) techniques.[27] For the one-step method, however, the current AlON powders often have unstable properties because of the instability of the preparation process, which makes the whole AlON transparent ceramics preparation process difficult to control.[28] Until now, highly transparent AlON ceramics have usually only been produced using a two-step synthesis process.[29−31]

In this paper, the wideband low loss aesthetically decorative ceramics DRA is designed. The ceramic DRA has a transparent rectangular block shape in which the interior has a laser engraved school logo. In addition, AlON transparent ceramics are prepared by carbothermal reduction nitriding of pure AlON powder and sintered under cold isostatic pressing. It is to be noted that in this work, the prepared AlON transparent ceramic has excellent microwave dielectric properties, making it a good candidate for application in the design of DRAs. At the same time, an indoor aesthetically decorative Wi-Fi DRA is designed for incorporation into the concept of a smart home.

RESULTS AND DISCUSSIONS

Figure 3a displays the XRD patterns of AlON transparent ceramic samples sintered at their optimum temperatures. It is clearly observed that all the diffraction peaks can be attributed to the standard AlON cubic spinel phase (JCPDS: #48−0686), and no secondary phase was detected.[32] The schematics of the crystal structure are shown in inset of the Figure 3a. The AlON transparent ceramic was sintered bodies with La_2O_3 sintering aids in cold isostatic pressing. As can be seen, after the AlON transparent ceramic sample was thermally etched, the microstructure and grain boundaries of the crystal grains can be observed. Figure 3b is an SEM image of AlON transparent ceramics. It can be seen from the figure that the microstructure of the sintered body is uniform; there are no pore or impurities between the insides of the crystal grains and the crystal grains, and the mean grain size of the AlON transparent ceramic sample is 264 μm. Meanwhile, AlON transparent ceramic samples have high transparency, and the transmittance curve is shown in Figure 3c. It can be observed from the figure that when the thickness of the AlON transparent ceramic sample is 9.0 mm, the sample has a good transmittance in the wavelength regions of 0.2 to 5.4 μm, and the transmittance in the wavelength regions of 0.35 to 4.0 μm can reach 83%.

The AlON transparent ceramics not only have good strength and stable chemical properties but also optimum microwave dielectric properties with a dielectric constant of ~9.32, Qf ~ 47 960 @ 8.25 GHz. Among them, the dielectric constant and loss tangent of the ceramic sample are calculated using the closed-cavity resonance method. This measuring system (Figure

Figure 2. Schematic diagram of the experimental synthesis strategy of the AlON transparent ceramic sample.

https://doi.org/10.1021/acsami.1c12223
ACS Appl. Mater. Interfaces 2021, 13, 46866−46874

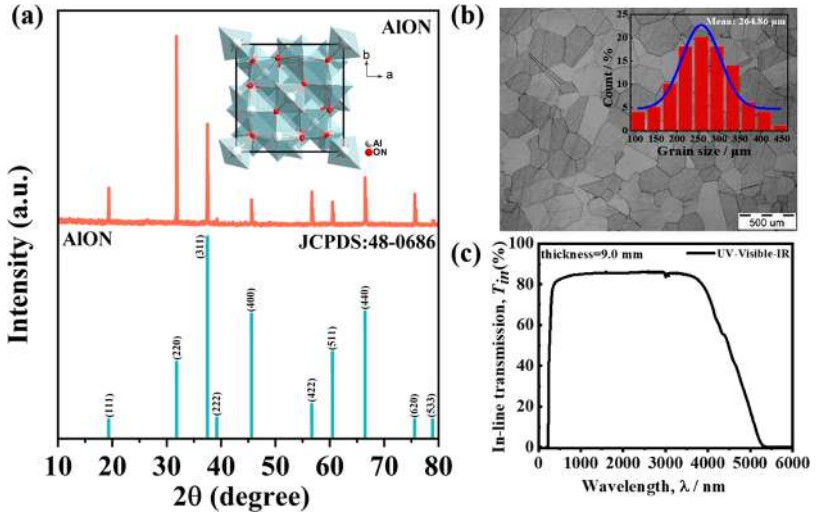

Figure 3. (a) X-ray diffraction patterns of AlON ceramic samples sintered at 1780 °C (inset is a schematic representation of the crystal structure of AlON ceramic). (b) SEM image and grain distribution size statistics of transparent ceramic samples. (c) In-line transmittance of the AlON transparent ceramic sample at UV−vis−NIR wavelengths.

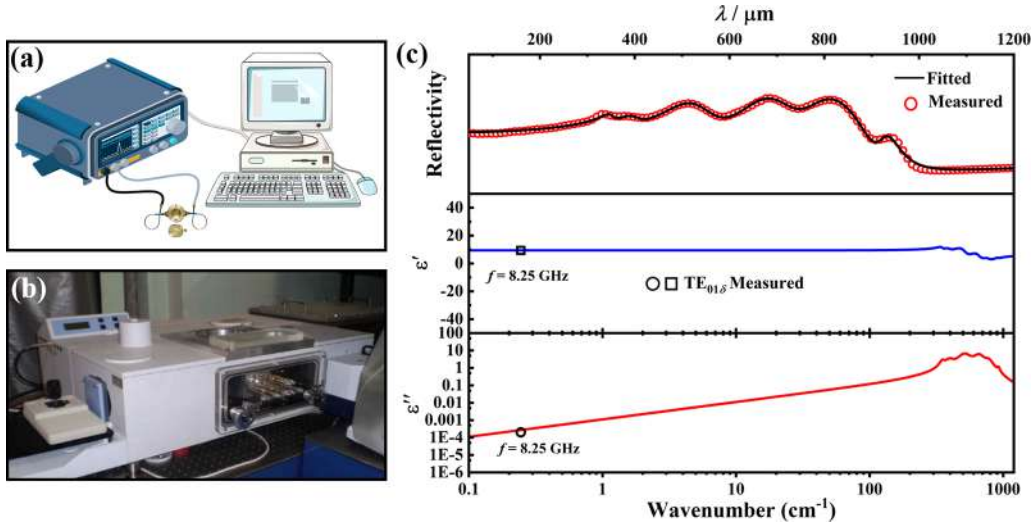

Figure 4. (a) Schematic diagram of resonant cavity measurement of dielectric properties. (b) Schematic diagram of infrared beamline measurement of far-infrared spectra. (c) Measured and fitted infrared reflectance spectroscopy (solid line stands for fitted, circle represents the measurement) and fitted complex dielectric spectra of AlON transparent ceramic samples (square and circle represent the closed-cavity test).

4a) commonly uses the Rayleigh−Ritz method (RRM)[33] to collect sample resonance frequency (f_0) of the $TE_{01\delta}$ mode, and then calculates the relative permittivity (ε_r) and loss tangent (tan δ) of the transparent ceramics by the size and f_0 of sample.

A classical harmonic oscillator model (see eq 1) was used to analyze the infrared reflectance spectra of the AlON transparent ceramic sample to further study its inherent microwave dielectric properties.

$$\varepsilon^*(\omega) = \varepsilon(\infty) + \sum_{j=1}^{n} \frac{(z_j e)^2 / m_j V_j \varepsilon_0}{\omega_{Tj}^2 - \omega^2 - j\gamma_j\omega} = \varepsilon(\infty) + \sum_{j=1}^{n} \frac{\omega_{Pj}^2}{\omega_{Tj}^2 - \omega^2 - j\gamma_j\omega} \quad (1)$$

The detailed explanation of the associated symbols in the above equation can refer to the previous literature.[34] Meanwhile, the relationship between complex reflectivity and relative permittivity can be expressed as

$$R(\omega) = \left| \frac{1 - \sqrt{\varepsilon(\omega)}}{1 + \sqrt{\varepsilon^*(\omega)}} \right|^2 \quad (2)$$

As it is in the microwave frequency band $\omega \ll \omega_{pj}$, the far-infrared reflection spectrum of the sample has a good fitting. Therefore, according to formula 3, the real and imaginary parts of the dielectric constant of AlON transparent ceramic can be easily obtained.

$$\varepsilon'(\omega) = \varepsilon(\infty) + \sum_{j=1}^{n} \frac{\omega_{Pj}^2}{\omega_{Tj}^2} = \varepsilon(\infty) + \sum_{j=1}^{n} \partial\varepsilon_j$$

$$\varepsilon''(\omega) = \omega \sum_{j=1}^{n} \frac{\partial\varepsilon_j\gamma_j}{\omega_{Tj}^2} \quad (3)$$

https://doi.org/10.1021/acsami.1c12223
ACS Appl. Mater. Interfaces 2021, 13, 46866−46874

For most microwave dielectric ceramics, the dielectric constant (ε_r) in the microwave frequency region is mainly determined by electronic displacement polarization and ionic displacement polarization. Among them, the optical frequency dielectric constant produced by electronic displacement polarization is $\varepsilon(\infty)$. As shown in Figure 4c, the infrared reflection spectrum of AlON ceramic samples at room temperature could be appropriately fitted by using six Lorentzian modes. Table 1 lists the phonon parameters corresponding to AlON transparent ceramics in Lorentzian modes as representative data. Furthermore, Figure 4c also shows the fitted spectrum of the complex permittivity. Meanwhile, as shown in Figure 4c, the experimental value obtained by the $TE_{01\delta}$ method is consistent with the calculated value of the complex permittivity obtained by fitting the far-infrared spectrum. This phenomenon indicates that in the microwave region, the polarization of dielectric ceramics is mainly caused by the absorption of phonons in the infrared region.[17]

Table 1. Phonon Parameters Obtained from the Fitting of the Far-Infrared Reflectivity Spectra of the AlON Transparent Ceramic Sample

mode	ω_{oj}	ω_{pj}	γ_j	ΔE_j
1	350.01	130.99	32.64	0.14
2	397.30	223.15	64.34	0.32
3	516.59	589.93	119.23	1.3
4	661.09	655.42	130.73	0.98
5	779.33	443.03	120.97	0.32
6	922.34	142.79	46.26	0.02
AlON	$\varepsilon_\infty = 2.49$		$\varepsilon_0 = 9.32$	

The AlON transparent ceramics have excellent microwave dielectric properties and high transparency. We propose a 5 GHz Wi-Fi aesthetically decorative DRA, as shown in Figure 5. It is composed of a rectangular transparent decorative ceramic DR and a metal ground on one side of the substrate, and a microstrip line aperture coupling feed structure is formed on the other side of the substrate. Among them, the aesthetically decorative DR was made by laser internal engraving the Jiao Tong University logo pattern inside the transparent ceramic. The length, width, and height of the aesthetically decorative DR ($\varepsilon_{r,DR} = 9.32$; tan $\delta = 1.72 \times 10^{-4}$) are a, b, and h, respectively. And the decorative DR would be mounted on the aperture position etched in the center of a Rogers-5880 grounding ($\varepsilon_{r,sub} = 2.2$; tan $\delta = 0.0009$) of thickness d that was purchased from Ao-ling Electronic Technology Co. Ltd. The dimensions of the microstrip-line and aperture are shown in Figure 5b, c, one end of the microstrip stretches to the edge of the Rogers-5880 printed circuit board, and a 50 Ω 2.92 mm connector is used at the end of the microstrip line for excitation. On the basis of this arrangement, the 5 GHz Wi-Fi decorative DRA was designed in commercial software *CST Microwave Studio* and is simulated through FDTD solver, and the final optimized parameters are shown in Table 2.

Table 2. Optimized Parameter Values

param	value (mm)	param	value (mm)
a	16.0	w_m	4.7
b	10.9	l_m	4.5
h	16.0	d	1.524
l_s	9.2	l	40.0
w_s	2.2	-	-

In this part, first, a single rectangular DR with a height of $2h$ was studied through image theory.[35] Meanwhile, rectangular DRA have been modeled as the dielectric waveguide model (DWM)[36] to find their resonance frequencies of the rectangular DRA. For a rectangular DRA having a dielectric constant of ε_r and dimensions of a, b, and h mounted on a perfect infinite ground plane, the resonant frequency f_{mn} of the TE^x_{mnl} mode, among them, the m, n, and l stand for the number of extreme values in the x-, y-, and z-directions, respectively. The characteristic equations of the wavenumbers K_x, K_y, and K_z for the TE^x_{mnl} mode can be derived using Maratelli's approximation technique[37] as in the following equation

$$k_x a = m\pi - 2\tan^{-1}(k_x/\varepsilon_r/k_{x0})$$
$$k_{x0} = [(\varepsilon_r - 1)k_0^2 - k_x^2]^{1/2} \quad (4)$$
$$k_y b = n\pi - 2\tan^{-1}(k_y/\mu_r/k_{y0})$$
$$k_{y0} = [(\varepsilon_r - 1)k_0^2 - k_y^2]^{1/2} \quad (5)$$

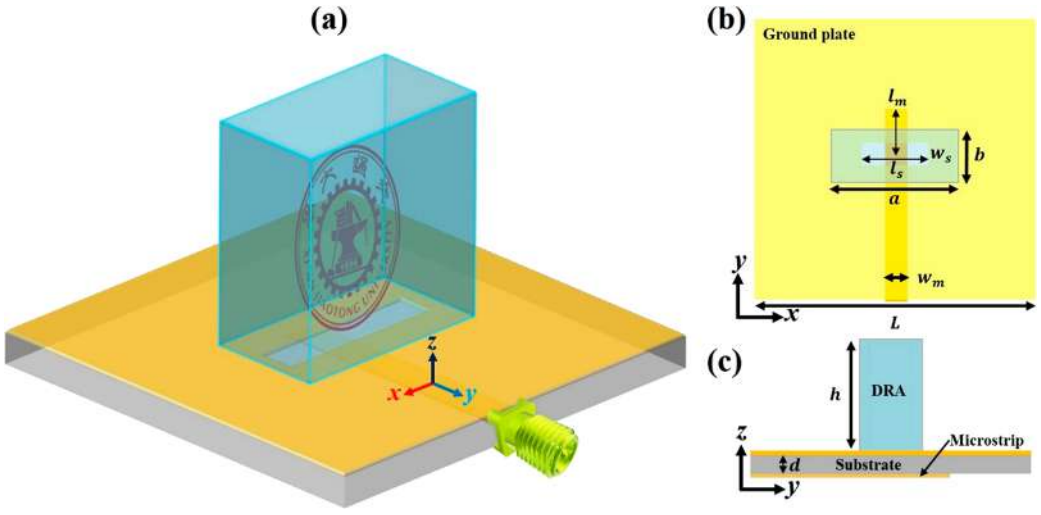

Figure 5. Configuration of the aesthetically decorative DRA. (a) 3D view. (b) Top view. (c) Side view.

https://doi.org/10.1021/acsami.1c12223
ACS Appl. Mater. Interfaces 2021, 13, 46866−46874

$$2k_z h = l\pi - 2\tan^{-1}(k_z/\varepsilon_r/k_{z0})$$

$$k_{z0} = [(\varepsilon_r - 1)k_0^2 - k_z^2]^{1/2} \quad (6)$$

where K_{x0}, K_{y0}, and K_{z0} are decay constants of the field outside the DRA, and K_0 is the free space wavenumber that can be determined from the $K_x^2 + K_y^2 + K_z^2 = \varepsilon_r k_0^2$.

The radiation Q factor of rectangular DRA can be calculated using[9] the following equation

$$Q = \frac{2\omega W_e}{P_{rad}} \quad (7)$$

where P_{rad} and W_e are radiated power and stored energy, respectively, and $\omega = 2\pi f_0$. The radiated power and stored energy are given by the following formulas

$$W_e = \frac{\varepsilon_0 \varepsilon_r ahbA^2}{32} \times \left[1 + \frac{\sin(k_x b)}{k_x b} \times (k_y^2 + k_z^2)\right] \quad (8)$$

$$P_{rad} = 10k_0^4 \left| \frac{-j\omega 8\varepsilon_0(\varepsilon_r - 1)A}{k_x k_y k_z} \sin(k_x d/2)\hat{x} \right|^2 \quad (9)$$

where A is a constant related to the maximum amplitude of the fields. For the DRA present in Figure 5, which would have value of $b = 10.9$ and $\varepsilon_r = 9.32$ at $a/h = 1$, the value of radiation factor $Q \approx 7.11$ can be calculated according to formulas 7 and 8.

It is shown that the aesthetically decorative rectangular DRA resonates at two frequencies 4.72 and 5.71 GHz in the desired frequency band, as shown in Figure 6a. In Figure 6b, the resistance and reactance curves of the aesthetically decorative DRA configuration are studied. With reference to the figure, it can be found that the corresponding resistance values at the two resonance frequencies of 4.72 and 5.71 GHz are almost equal to 50 Ω, and the reactance at the two resonance frequencies is also almost 0 Ω, which indicates that the proposed DRA has good impedance matching in the entire operating frequency band.

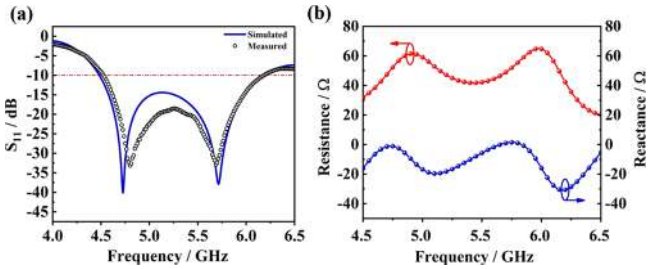

Figure 6. (a) Measured (black circle) and simulated (blue solid line) reflection coefficient S_{11} of the aesthetically decorative DRA. (b) Resistance and reactance values over the band for the aesthetically decorative DRA configuration.

To verify the corresponding resonance modes, we depict the *E*-field volume distribution inside the rectangular DRA at the resonances in Figure 7a, b. With reference to the figure, it can be found that the *E*-field distribution patterns inside the DRA at two resonance frequencies. Meanwhile, to more clearly show the *E*-field distribution, the field distribution of the *yoz*-plane is shown in Figure 7c. The resonance frequency corresponding to the fundamental TE^x_{111} mode is 4.72 GHz and the higher-order TE^x_{113} mode is 5.71 GHz. This indicates the possibility of linear polarization with low cross-polarization. In addition, in Figure 7c, the electric field vector is perpendicular to the ground plane. This should be the case because the ground plane is believed to be a perfect conductor.[38] As a result, the dominant mode (TE^x_{111}) and high-order mode (TE^x_{113}) of the aesthetically decorative AlON transparent ceramic dielectric resonator is excited to realize a broadband 5 GHz Wi-Fi DRA. Meanwhile, Figure 9c shows a prototype of the proposed aesthetically decorative DRA. The simulated and measured S-parameters of the antenna are shown in Figure 6a, showing good agreement. The simulated <−10 dB impedance bandwidth is 32% (4.48−6.19 GHz). The measured <−10 dB impedance bandwidth is approximately 31.4%, ranging from 4.51−6.19 GHz. Additionally, the aesthetically decorative DRA is designed to operate over the 5 GHz Wi-Fi band of 4.9−5.9 GHz.[39] And the weak defects caused by the laser inner engraving logo pattern have no effect on the antenna performance.

The radiation performances of the fabricated antenna are measured by the Satimo *StarLab* system. Figure 9b shows the antenna measurement setup. Figure 8e, f shows the 3D radiation patterns of copolarization and cross-polarization for the DRA at 4.72 and 5.71 GHz. Figure 8a−d shows the simulated and measured normalized radiation patterns in the *xoz*-plane and *yoz*-plane at 4.72 and 5.71 GHz. For the *H*-plane (*xoz*-plane) and *E*-plane (*yoz*-plane) patterns, in the boresight direction ($\theta = 0°$) of the axis, the copolarized fields is more than 30 dB stronger than the cross-polarized fields. Ultimately, the measured results of the normalized radiation patterns are in good agreement with the simulated results.

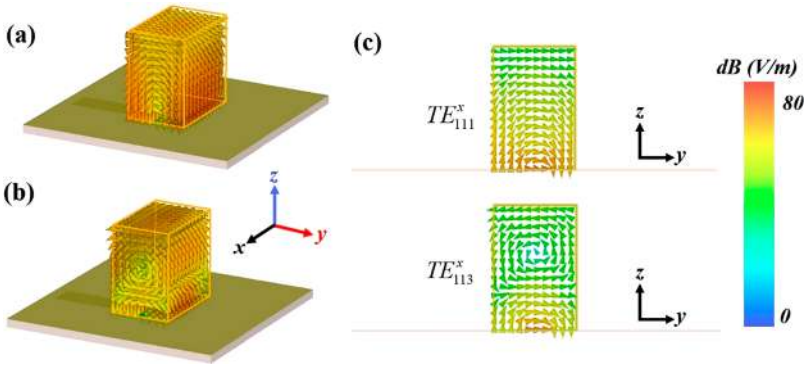

Figure 7. *E*-field volume distribution of the aesthetically decorative DRA at (a) 4.72 GHz and (b) 5.71 GHz. (c) *E*-field distribution of TE^x_{111} mode (4.72 GHz) and TE^x_{113} mode (5.71 GHz) in the *yoz*-plane.

https://doi.org/10.1021/acsami.1c12223
ACS Appl. Mater. Interfaces 2021, 13, 46866−46874

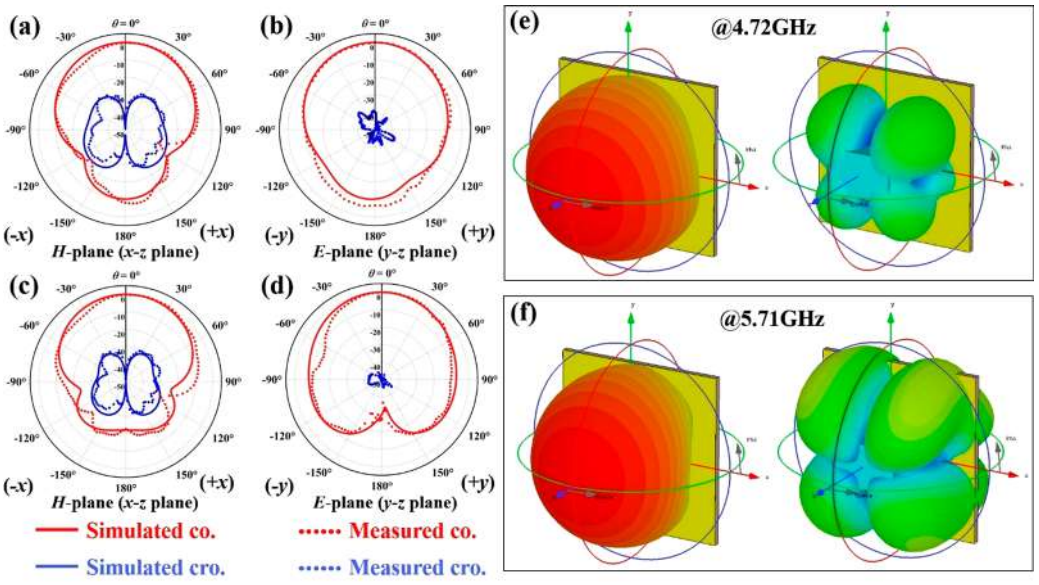

Figure 8. Normalized radiation pattern of the measured (dashed line) and simulated (solid line) AlON ceramic decorative DRA. (a) *xoz*-plane and (b) *yoz*-plane are the radiation patterns at the resonance frequency of 4.72 GHz (TE^{x}_{111}). (c) *xoz*-plane and (d) *yoz*-plane are radiation patterns at a resonance frequency of 5.71 GHz (TE^{x}_{113}). 3D radiation patterns of copolarized and cross-polarized for the DRA at (e) 4.72 GHz and (f) 5.71 GHz.

Figure 9a shows the realized gain and radiation efficiency of the proposed aesthetically decorative DRA. The simulated and measured results both show that the proposed antenna has a stable realized gain of approximately 6.50 dBi over the entire 5 GHz Wi-Fi bandwidth and a peak gain is 6.79 dBi at 5 GHz. In general, the measured results are in good agreement with the simulated results. At the same time, Figure 9a depicts the simulated and measured the radiation efficiency of the aesthetically decorative DRA. The measured radiation efficiency is approximately larger than 85% at the entire 5 GHz Wi-Fi bandwidth. Obviously, it can be found from the figure that the measured radiation efficiency is lower than the simulation results, which is mainly caused by the interconnection between the measuring instrument and the antenna prototype and the insertion loss of the feed network.[40] It can be found in Table 3 that most reported Wi-Fi antenna materials are normally SiO_2 glass or dielectrics with high loss and deteriorative dispersion. Because of the low loss and deteriorative dispersion effect, this will result in low radiation efficiency and high cross-polarization of the antennas. Meanwhile, a suitable dielectric constant can also excite the high-order mode of the rectangular DRA, which can achieve a wide impedance bandwidth. Compared to the DRA performance in Table 3, the AlON transparent ceramic DRA not only has high radiation efficiency and wide bandwidth but also low cross-polarization.

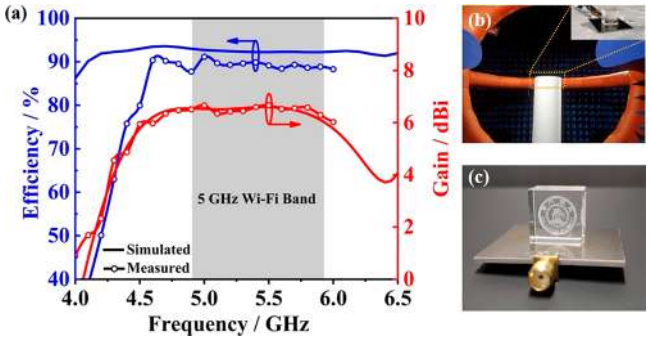

Figure 9. (a) Simulated and measured realized gain (red line) and radiation efficiency (blue line) of the proposed aesthetically decorative DRA. (b) SATIMO multiprobe antenna near-field measurement system. (c) Photograph of the fabricated aesthetically decorative DRA prototype.

Table 3. Performance Comparison of Different DRA Materials for the Wi-Fi Antenna Applications[a]

DR materials	ε_r	tan δ	dispersion	BW (%)	XPD (dB)	refs
K-9 glass	7.00	0.002	high	13.5	−23	10
Li_2O-ZnO-GeO_2	8.15	1.75×10^{-4}	low	7	−5	4
glass	6.85	0.002	high	28	−20	11
dielectric	12	N/A	high	14	−25	2
AlON	9.32	1.72×10^{-4}	low	32	−30	this work

[a]BW, bandwidth; XPD, cross-polarization discrimination.

Finally, the proposed 5 GHz Wi-Fi aesthetically decorative DRA prototype is shown in Figure 9c. Using high-quality-factor AlON transparent ceramics, the aesthetically decorative DRA exhibits a high radiation efficiency (Figure 9a) and low cross-polarization (Figure 8). In addition, when the proposed antenna and some previously reported 5 GHz Wi-Fi antennas are compared,[4,5,41,42] the proposed antenna exhibits not only a high radiation efficiency and low cross-polarization but also is an indoor aesthetically decorative Wi-Fi DRA that is designed to incorporate well into the concept of a smart home.

CONCLUSIONS

In summary, the AlON transparent ceramics are successfully prepared via a cold-isostatic-pressed reaction. First, according to XRD analysis, the measured results indicate that the diffraction peaks of AlON ceramics could be indexed to a standard AlON cubic spinel phase. Then, based on the measurement data of the microwave dielectric properties, the optimum dielectric properties of $\varepsilon_r \sim 9.32$, $Qf \sim 47\,960$ are obtained in the AlON transparent ceramic by cold isostatic pressing. Furthermore, the

https://doi.org/10.1021/acsami.1c12223
ACS Appl. Mater. Interfaces 2021, 13, 46866−46874

AlON transparent ceramic can also have a good chemical stability and higher transmittance (from 0.35 to 4.0 μm can reach 83%). Finally, a novel kind of aesthetically decorative 5 GHz Wi-Fi DRA has been designed by an AlON transparent ceramic, which has several advantages such as high radiation efficiency and low cross-polarization. And in order to achieve broad bandwidth, the proposed the antenna was excited in its dominant TE^{x}_{111} mode and higher-order TE^{x}_{113} mode. On the basis of Leung et al.'s breakthrough in using quartz glass as a decorative antenna, we further verified the application of transparent microwave dielectric ceramics in the direction of decorative antennas. The proposed antenna is thus an excellent candidate for an indoor aesthetically decorative Wi-Fi antenna.

EXPERIMENTAL SECTION

Sample Synthesis. The raw material used to prepare AlON is high-purity γ-Al_2O_3 (purity >99.97%, Dalian Highland Materials Co., Ltd., China), and carbon black (purity >97.5%, Sinopharm Reagent Co. Ltd., China), which were used as precursor materials and 0.08 wt% Y_2O_3 (99.99%, Aladdin Reagent Co. Ltd., China) and 0.05 wt% La_2O_3 (99.99%, Aladdin Reagent Co. Ltd., China) were codoped as sintering aids. γ-Al_2O_3 and carbon black were dispersed in an ethanol solution and ball milled for 20 h. The resulting precursor slurry was dried at 60 °C for 24 h.

The dried precursor was sieved through a 100-mesh nylon screen, and then heated at 1780 °C for 4 h in a graphite furnace under the protection of a N_2 atmosphere to synthesize AlON powder. The residual carbon black was removed at 600 °C in air for 2 h. The AlON powder was sieved through a 100-mesh nylon screen and ball milled with Y_2O_3 and La_2O_3 in an ethanol solution at a speed of 270 rpm for 20 h. The dried mixture was pressed into a disk at a speed of 5 MPa/min. The disk was subjected to cold isostatic pressing (CIP) at a speed of 200 MPa/5 min. The treated disc was then sintered in a graphite furnace at 1950 °C for 30 h under the protection of a N_2 atmosphere. The samples were machined and optically polished on two sides. Figure 2 shows a schematic diagram of the experimental process of AlON transparent ceramics.

Sample Characterizations. The crystal structure of the sample was analyzed with an X-ray diffractions (XRD) patterns which was applied using Cu Kα radiation; the 2θ degree ranged from 10 to 80° at 0.02 step size. Use the scanning electron microscopy (SEM, Model: Quanta F250) to observe the microstructures of the specimens and use the Nano Measurer software to calculate the average grain size from the SEM image of the sample. The transmittances of AlON transparent ceramic samples were tested through an ultraviolet−visible near-infrared (UV−vis-NIR) spectrophotometer (Cary 5000, Varian, Seattle, USA). The far-infrared spectrum of the AlON transparent ceramic sample was tested on the infrared ray-line of the Hefei National Synchrotron Radiation Laboratory. The dielectric properties at microwave frequencies were tested by $TE_{01\delta}$ dielectric resonator method[33] using a network analyzer (HP8720ES, Agilent). The *TCF* test from 25°C to 85°C was carried out in a Delta 9023 incubator and its calculation is expressed by equation 10.

$$\mathrm{TCF}(\tau_f) = \frac{f_{85} - f_{25}}{f_{25}(85 - 25)} \times 10^6 \tag{10}$$

where f_{25} and f_{85} are the $TE_{01\delta}$ resonant frequencies at 25°C and 85°C, respectively.

Antenna Characterizations. Aesthetic decorative resonator by laser internal engraving of the Jiao Tong University logo pattern inside a transparent dielectric ceramic. The design and optimization of DRA was done by the commercial software *CST Microwave Studio*. Meanwhile, antenna measurements are conducted in a microwave anechoic chamber using the Satimo *Stralab* system test method.

AUTHOR INFORMATION

Corresponding Authors

Di Zhou − *Multifunctional Materials and Structures, Key Laboratory of the Ministry of Education, School of Electronic Science and Engineering, Xi'an Jiaotong University, Xi'an, Shaanxi 710049, China;* orcid.org/0000-0001-7411-4658; Email: zhoudi1220@gmail.com

He-Tuo Chen − *State Key Laboratory of High Performance Ceramics and Superfine Microstructure, Shanghai Institute of Ceramics, Chinese Academy of Sciences, Shanghai 200050, China; CAS Key Laboratory of Transparent Opto-functional Inorganic Materials, Shanghai Institute of Ceramics, Chinese Academy of Sciences, Shanghai 201899, China;* Email: chenhetuo@mail.sic.ac.cn

Ming-Zhao Dang − *Guangdong Fenghua Advanced Technology Holding Co., Ltd, Zhaoqing, Guangdong 526000, China;* Email: dmzwtt@qq.com

Authors

Chao Du − *Multifunctional Materials and Structures, Key Laboratory of the Ministry of Education, School of Electronic Science and Engineering, Xi'an Jiaotong University, Xi'an, Shaanxi 710049, China*

Shu-Zhao Hao − *Multifunctional Materials and Structures, Key Laboratory of the Ministry of Education, School of Electronic Science and Engineering, Xi'an Jiaotong University, Xi'an, Shaanxi 710049, China*

Jian Zhang − *State Key Laboratory of High Performance Ceramics and Superfine Microstructure, Shanghai Institute of Ceramics, Chinese Academy of Sciences, Shanghai 200050, China; CAS Key Laboratory of Transparent Opto-functional Inorganic Materials, Shanghai Institute of Ceramics, Chinese Academy of Sciences, Shanghai 201899, China*

Shi-Kuan Sun − *School of Material Science and Energy Engineering, Foshan University, Foshan, Guangdong 528000, China*

Tao Zhou − *School of Electronic and Information Engineering, Hangzhou Dianzi University, Hangzhou 310018, China*

Shao-Fei Wang − *School of Electronic and Information Engineering, Xi'an Jiaotong University, Xi'an 710049, China*

Hai-Wen Liu − *School of Electronic and Information Engineering, Xi'an Jiaotong University, Xi'an 710049, China*

Long Li − *School of Electronic Engineering, and the Collaborative Innovation Center of Information Sensing and Understanding, Xidian University, Xi'an 71007, China;* orcid.org/0000-0003-0472-7314

Zhuo Xu − *Multifunctional Materials and Structures, Key Laboratory of the Ministry of Education, School of Electronic Science and Engineering, Xi'an Jiaotong University, Xi'an, Shaanxi 710049, China*

Complete contact information is available at: https://pubs.acs.org/10.1021/acsami.1c12223

Author Contributions

D.Z. and C.D.: carried out laboratory research, wrote draft of manuscript; S.Z.H., H.T.C., and M.Z.D.: carried out characterization of microstructural; S.F.W., H.W.L., and L.L.: carried out characterization of antenna performance; S.K.S., J.Z., T.Z., and Z.X.: contributed to the writing and revisions.

Notes

The authors declare no competing financial interest.

https://doi.org/10.1021/acsami.1c12223
ACS Appl. Mater. Interfaces 2021, 13, 46866−46874

■ ACKNOWLEDGMENTS

This work was supported by the National Natural Science Foundation of China (51972260, 52072295), the International Cooperation Project of Shaanxi Province (2021KWZ-10), the open project of State Key Laboratory of Advanced Materials and Electronic Components (FHR-JS-202011003), the Fundamental Research Funds for the Central University (Grant xzy022020046), the 111 Project of China (B14040), and the Natural Science Foundation of Shanghai (Grant 19ZR1465000).

■ REFERENCES

(1) Zhang, J.; Wei, B.; Wu, F. X.; Dong, L. M.; Hu, W.; Kanhere, S. S.; Luo, C. W.; Yu, S.; Cheng, J. Gate-ID: WiFi-Based Human Identification Irrespective of Walking Directions in Smart Home. *IEEE Internet Things J.* **2021**, *8*, 7610−7624.

(2) Li, B.; Liao, S. W.; Xue, Q. Omnidirectional Circularly Polarized Antenna Combining Monopole and Loop Radiators. *IEEE Antennas and Wireless Propagation Letters* **2013**, *12*, 607−610.

(3) Zhang, Z. Y.; Fu, G.; Wu, W. J.; Lei, J.; Gong, S. X. A Wideband Dual-Sleeve Monopole Antenna for Indoor Base Station Application. *IEEE Antennas and Wireless Propagation Letters* **2011**, *10*, 45−48.

(4) Xiang, H.; Kilpijärvi, J.; Myllymäki, S.; Yang, H.; Fang, L.; Jantunen, H. Spinel-Olivine Microwave Dielectric Ceramics with Low Sintering Temperature and High Quality Factor for 5 GHz Wi-Fi Antennas. *Applied Materials Today* **2020**, *21*, 100826−100834.

(5) Deng, C. j.; Lv, X.; Feng, Z. H. High Gain Monopole Antenna with Sleeve Ground Plane for WLAN Applications. *IEEE Antennas and Wireless Propagation Letters* **2017**, *16*, 2199−2202.

(6) Long, S.; Mcallister, M.; Shen, L. The Resonant Cylindrical Dielectric Cavity Antenna. *IRE Trans. Antennas Propag.* **1983**, *31* (3), 406−412.

(7) Chaudhuri, S.; Mishra, M.; Kshetrimayum, R. S.; Sonkar, R. K.; Chel, H.; Singh, V. K. Rectangular DRA Array for 24 GHz ISM-Band Applications. *IEEE Antennas and Wireless Propagation Letters* **2020**, *19* (9), 1501−1505.

(8) Ng, H. K.; Leung, K. W. *Dielectric Resonator Antennas*; John Wiley & Sons, Inc.: 2003.

(9) Petosa, A. *Dielectric Resonator Antenna Handbook*. Artech house publish, 2007.

(10) Leung, K.W.; Lim, E. H.; Fang, X. S. Dielectric Resonator Antennas: From the Basic to the Aesthetic. *Proc. IEEE* **2012**, *100* (7), 2181−2193.

(11) Leung, K. W.; Pan, Y. M.; Fang, X. S.; Lim, E. H.; Luk, K. M.; Chan, H. P. Dual-Function Radiating Glass for Antennas and Light Covers—Part I: Omnidirectional Glass Dielectric Resonator Antennas. *IEEE Trans. Antennas Propag.* **2013**, *61* (2), 578−586.

(12) Leung, K. W.; Fang, X. S.; Pan, Y. M.; Lim, E. H.; Luk, K. M.; Chan, H. P. Dual-Function Radiating Glass for Antennas and Light Covers—Part II: Dual-Band Glass Dielectric Resonator Antennas. *IEEE Trans. Antennas Propag.* **2013**, *61* (2), 587−597.

(13) Maguire, E. A.; Rawson, J. K.; Tustison, R. W. Aluminum Oxynitride's Resistance to Impact and Erosion. *Proc. SPIE* **1994**, *2286*, 2286−2291.

(14) Sova, R. M.; Linevsky, M. J.; Thomas, M. E.; Mark, F. F. High-Temperature Infrared Properties of Sapphire, AlON, Fused Silica, Yttria, and Spinel. *Infrared Phys. Technol.* **1998**, *39* (4), 251−261.

(15) Hartnett, T. M.; Bernstein, S. D.; Maguire, E. A.; Tustison, R. W. Optical Properties of ALON (Aluminum Oxynitride). *Infrared Phys. Technol.* **1998**, *39*, 203−211.

(16) Goldman, L. M.; Balasubramanian, S.; Kashalikar, U.; Foti, R.; Sastri, S. Scale up of Large AlON Windows. *Proc. SPIE* **2013**, *8708*, 870804.

(17) Guo, H. H.; Zhou, D.; Du, C.; Wang, P. J.; Liu, W. F.; Pang, L. X.; Wang, Q. P.; Su, J. Z.; Singh, C.; Trukhanov, S. Temperature Stable $Li_2Ti_{0.75}(Mg_{1/3}Nb_{2/3})_{0.25}O_3$-Based Microwave Dielectric Ceramics with Low Sintering Temperature and Ultra-Low Dielectric Loss for Dielectric Resonator Antenna Applications. *J. Mater. Chem. C* **2020**, *8* (14), 4690−4700.

(18) Chen, Z.; Shen, C.; Liu, H.; Ye, X.; Qi, L.; Yao, Y.; Yu, J.; Chen, X. Millimeter-Wave Rectangular Dielectric Resonator Antenna Array with Enlarged DRA Dimensions, Wideband Capability, and High-Gain Performance. *IEEE Trans. Antennas Propag.* **2020**, *68* (4), 3271−3276.

(19) Du, C.; Guo, H. H.; Zhou, D.; Chen, H. T.; Zhang, J.; Liu, W. F.; Su, J. Z.; Liu, H. W. Dielectric Resonator Antennas Based on High Quality Factor $MgAl_2O_4$ Transparent Dielectric Ceramics. *J. Mater. Chem. C* **2020**, *8* (42), 14880−14885.

(20) Shannon, R. D. Dielectric Polarizabilities of Ions in Oxides and Fluorides. *J. Appl. Phys.* **1993**, *73* (1), 348−366.

(21) Warner, C. T.; Hartnett, T. M.; Fisher, D.; Sunne, W. Characterization of AlON Optical Ceramic. *Proc. SPIE* **2005**, *57* (86), 95−111.

(22) Hartnett, T. M.; Bernstein, S. D.; Maguire, E. A.; Tustison, R. W. Optical Properties of AlON (aluminum oxynitride). *Proc. SPIE* **1997**, 284−295.

(23) Chen, F.; Zhang, F.; Wang, J.; Zhang, H. L.; Tian, R.; Zhang, J.; Zhang, Z.; Sun, F.; Wang, S. W. Microstructure and Optical Properties of Transparent Aluminum Oxynitride Ceramics by Hot Isostatic Pressing. *Scr. Mater.* **2014**, *81*, 20−23.

(24) Kang, B.; Kang, S. Crystallization Behavior and Optical Properties of Glass-Ceramics Containing Nano-Diopside Crystals. *Sci. Adv. Mater.* **2020**, *12*, 510−515.

(25) Zhang, N.; Liang, B.; Wang, X. Y.; Kan, H. M.; Zhu, K. W.; Zhao, X. J. The Pressureless Sintering and Mechanical Properties of AlON Ceramic. *Mater. Sci. Eng., A* **2011**, *528* (19−20), 6259−6262.

(26) Mccauley, J. W.; Corbin, N. D. Phase Relations and Reaction Sintering of Transparent Cubic Aluminum Oxynitride Spinel (AlON). *J. Am. Ceram. Soc.* **1979**, *62* (9−10), 476−479.

(27) Willems, H.X.; Hendrix, M.M.R.M.; Metselaar, R.; de With, G. Thermodynamics of AlON I: Stability at Lower Temperatures. *J. Eur. Ceram. Soc.* **1992**, *10* (4), 327−337.

(28) Qi, J. Q.; Wang, Y. Z.; Lu, T. C.; Yu, Y.; Pan, L.; Wei, N.; Wang, J. Preparation and Light Transmission Properties of AlON Ceramics by the Two-Step Method with Nanosized Al_2O_3 and AlN. *Metall. Mater. Trans. A* **2011**, *42* (13), 4075−4079.

(29) Liu, Q.; Jiang, N.; Li, J.; Sun, K.; Pan, Y. B.; Guo, J. K. Highly Transparent AlON Ceramics Sintered from Powder Synthesized by Carbothermal Reduction Nitridation. *Ceram. Int.* **2016**, *42* (7), 8290−8295.

(30) Shan, Y. C.; Zhang, Z. H.; Sun, X. N.; Xu, J. J.; Qin, Q. H.; Li, J. T. Fast Densification Mechanism of Bimodal Powder During Pressureless Sintering of Transparent AlON Ceramics. *J. Eur. Ceram. Soc.* **2016**, *36* (3), 671−678.

(31) Sun, X. N.; Wu, H. K.; Zhu, G. Z.; Shan, Y. C.; Xu, J. J.; Li, J. T.; Olevsky, E. A. Direct Coarse Powder Aqueous Slip Casting and Pressureless Sintering of Highly Transparent AlON Ceramics. *Ceram. Int.* **2020**, *46* (4), 4850−4856.

(32) Corbin, N. D. Aluminum Oxynitride Spinel: A Review. *J. Eur. Ceram. Soc.* **1989**, *5* (3), 143−154.

(33) Krupka, J. Frequency Domain Complex Permittivity Measurements at Microwave Frequencies. *Meas. Sci. Technol.* **2006**, *17* (6), R55−R70.

(34) Guo, H. H.; Zhou, D.; Pang, L. X.; Qi, Z. M. Microwave Dielectric Properties of Low Firing Temperature Stable Scheelite Structured $(Ca,Bi)(Mo,V)O_4$ Solid Solution Ceramics for LTCC Applications. *J. Eur. Ceram. Soc.* **2019**, *39* (7), 2365−2373.

(35) Pan, Y. M.; Leung, K. W.; Luk, K. M. Design of the Millimeter-wave Rectangular Dielectric Resonator Antenna Using a Higher-Order Mode. *IEEE Trans. Antennas Propag.* **2011**, *59* (8), 2780−2788.

(36) Kumar Mongia, R.; Ittipiboon, A. Theoretical and Experimental Investigations on Rectangular Dielectric Resonator Antennas. *IEEE Trans. Antennas Propag.* **1997**, *45* (9), 1348−1356.

(37) Mongia, R. K. Theoretical and Experimental Resonant Frequencies of Rectangular Dielectric Resonators. *IEEE Proceedings Microwaves, Antennas and Propagation* **1992**, *139* (1), 98−104.

https://doi.org/10.1021/acsami.1c12223
ACS Appl. Mater. Interfaces 2021, 13, 46866−46874

(38) Al Salameh, M. S.; Antar, Y. M. M.; Seguin, G. Coplanar-Waveguide-Fed Slot-Coupled Rectangular Dielectric Resonator Antenna. *IEEE Trans. Antennas Propag.* **2002**, *50* (10), 1415−1419.
(39) Lin, F. H.; Chen, Z. N. Low-Profile Wideband Metasurface Antennas Using Characteristic Mode Analysis. *IEEE Trans. Antennas Propag.* **2017**, *65* (4), 1706−1713.
(40) Liu, H. W.; Tian, H. L.; Du, C.; Huang, T. T.; Zhao, Z. Y.; Zhou, D. Dual-Band Filtering Dielectric Antenna Using High-Quality-Factor $Y_3Al_5O_{12}$ Transparent Dielectric Ceramic. *Adv. Eng. Mater.* **2021**, *23*, 2100115−2100124.
(41) Darimireddy, N. K.; Reddy, R. R.; Prasad, A. M. Wideband Circularly Polarized Cylindrical Dielectric Resonator Antennas with Rectangular Curved Slots. *IEEE Antennas and Propagation Magazine* **2020**, *62* (6), 65−73.
(42) Mishra, S.; Das, S.; Pattnaik, S. S.; Kumar, S.; Kanaujia, B. K. Three-Dimensional Dual-Band Dielectric Resonator Antenna for Wireless Communication. *IEEE Access* **2020**, *8*, 71593−71604.

https://doi.org/10.1021/acsami.1c12223
ACS Appl. Mater. Interfaces 2021, 13, 46866−46874